JMEPEG (2012) 21:1085–1090
DOI: 10.1007/s11665-011-9980-6

1059-9495/$19.00

Residual Stresses in Microarc Oxidation Ceramic Coatings on Biocompatible AZ31 Magnesium Alloys

Yanhong Gu, Wenming Xiong, Chengyun Ning, and Jing Zhang

(Submitted February 21, 2011; in revised form April 16, 2011)

Ceramic coatings have been successfully prepared on biocompatible AZ31 magnesium alloy substrates using microarc oxidation (MAO) technique. Residual stresses attributed to the MgO constituent of the coatings at different oxidation voltages have been evaluated by x-ray diffraction using the $\sin^2 \psi$ method. It is found that tensile residual stresses were present in the coatings, and they decreased from 1418 to 545 MPa as the oxidation voltages increased from 250 to 350 V. Correlations between the residual stresses and microstructural morphology have been discussed. The residual stress characteristics are attributed to the microcracks and the new phase formation during the MAO process.

Keywords magnesium alloy, microarc oxidation, residual stresses, x-ray diffraction

1. Introduction

Magnesium alloys have become a new class of degradable biomaterials for orthopedic applications because of their excellent biocompatibilities (Ref 1-3). Additional attractive features of magnesium alloys include outstanding physical and mechanical properties, such as high strength and stiffness, low density, low elastic modulus, and good castability (Ref 1). However, magnesium alloys have a high corrosion rate, which is obviously a drawback with regard to biomedical applications (Ref 4, 5). Conventional preparation methods, such as anodic oxidation (Ref 6, 7), polymer coating (Ref 8), chemical conversion coating (Ref 9), plasma anodization (Ref 10), and magnetron sputtering process (Ref 11) do not produce satisfactory coatings, because the coatings produced by these methods have a low corrosion resistance.

Microarc oxidation (MAO) technique, also called as plasma electrolytic oxidation (PEO) method, has been developed recently as a promising solution to the low corrosion resistance problems (Ref 12-15). In MAO processes, the metal or alloy samples to be coated serve as anodes. The samples are immersed in a stainless steel bath as the cathode which contains the electrolyte, typically a dilute alkaline solution (Ref 16). When the MAO process is applied on magnesium alloy, oxidation voltage is typically about 200 V (Ref 12-15). This voltage exceeds the local dielectric breakdown potential of growing oxide film, and therefore discharges may occur. These discharges result in localized plasmas, producing a high temperature and pressure for producing dense oxide coatings.

During the MAO deposition process, residual stresses arise due to temperature and microstructural changes. Residual stresses have a great effect on various characteristics of the coatings, such as corrosion, fatigue, fracture, wear, and friction properties (Ref 17). Despite the importance of residual stress on the biological, physical, and mechanical performances of the MAO coatings, only a few studies have addressed this issue. Khan et al. studied the residual stress in MAO coatings on Al alloy (Ref 18). Their study showed that residual stresses in the MAO coatings were formed as a result of a complex interaction between stress-generation and stress-relaxation processes. Huang et al. investigated the mechanical properties of titania prepared by MAO at different voltages (Ref 19). Their study showed that residual stress increased with applied voltages. Previous studies were primarily focused on the microstructural characteristics and residual stress measurements of MAO coating on Al and Ti alloys. There is so far no study on residual stress studies of MAO coating on Mg alloy substrates.

In the study, the residual stresses in MAO coatings produced on AZ31 magnesium alloy substrates at various deposition voltages are reported. The stresses are evaluated using $\sin^2 \psi$ x-ray diffraction technique. Both the surface and cross-section of the coatings are examined using scanning electron microscopy. The effects of applied voltage on residual stresses are discussed. Finally, the correlation between the residual stress and microstructure is proposed.

2. Experimental

2.1 Preparation of the MAO Coatings

Square plates (20 mm × 20 mm × 1 mm) of AZ31 magnesium alloy with a chemical composition of 2.5-3.5 wt.% Al, 0.7-1.3 wt.% Zn, 0.2-1.0 wt.% Mn, 0.05 wt.% Si, 0.01 wt.% Cu, and Mg balance, were used as the substrates for coating deposition. Before MAO treatment, the substrates were mechanically polished to achieve a surface finish of Ra ≈ 1.6

Yanhong Gu and **Jing Zhang**, Department of Mechanical Engineering, University of Alaska Fairbanks, Fairbanks, AK 99775; and **Wenming Xiong** and **Chengyun Ning**, College of Materials Science and Engineering, South China University of Technology, Guangzhou 510640, People's Republic of China. Contact e-mail: jzhang6@alaska.edu.

μm, ultrasonically cleaned in ethanol for 5 min, and then dried. The coatings were prepared on the AZ31 magnesium alloy surfaces with a 50-kW capacity MAO equipment (MAO20, Chengdu PULSETECH Electrical Co., China). The equipment has an adjustable pulsed DC source, a stainless steel container with a sample holder as the electrolyte, and a stirring and cooling system. The magnesium alloy substrate and the wall of the stainless steel container were used as the anode and the cathode, respectively. An electrolyte prepared from a solution of 10 g/L Na_3PO_4 in distilled water was kept at room temperature during the entire treatment procedure. A pulsed current was applied at the frequency of 100 Hz, and the duty cycle of 0.3. The duty cycle is defined as the ratio between pulse duration and the period of a rectangular waveform. In order to study the effect of the applied voltage, coatings were produced at four different voltages, 250, 300, 325, and 350 V. for a constant 5-min deposition period.

2.2 Characterizations

2.2.1 Residual Stress Measurement. A x-ray diffractometer (X'Pert PRO MRD, PANalytical B.V., The Netherlands) with Cu Kα radiation (45 kV and 40 mA) was used for a detailed study of surface phase composition of the coatings. The samples were scanned at normal θ/2θ geometry in the 2θ range from 20° to 60° with 0.0125° size step.

Residual stresses in the MgO constituent of the coating were measured by the $\sin^2 \psi$ method (Ref 20):

$$\sigma_\phi = -\frac{E}{2(1+\nu)} \operatorname{ctg} \theta_0 \frac{\pi}{180} \frac{\partial(2\theta)}{\partial(\sin^2 \psi)} \quad \text{(Eq 1)}$$

where θ_0 is the Bragg's angle at diffraction peak in the samples without residual stress, θ is the Bragg's angle at diffraction peak in the samples with residual stress, E is Young's modulus, and ν is Poisson's ratio of the thin film. In this study, the elastic constants of MgO used were E = 248 GPa (Ref 21); and ν = 0.187 (Ref 21). In this study, the diffracted peak (200) at 2θ = 42.909° was used (θ_0 = 21.4545°). The measurements were carried out at four different ψ angles (0°, 15°, 30°, and 45°) in the 2θ range from 41° to 45° with a scan step of 0.0031° (2θ).

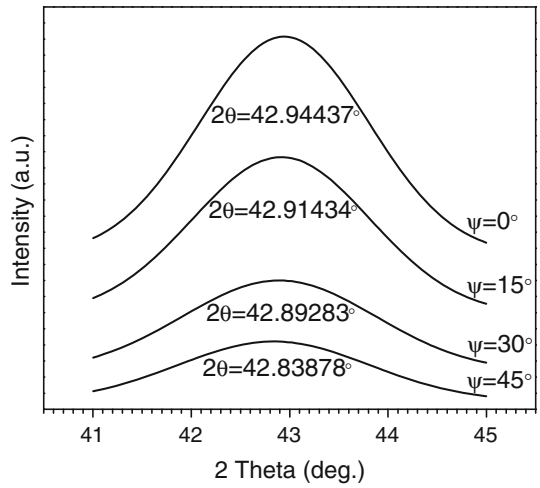

Fig. 1 An example of XRD spectrum shift at different ψ values for MAO-coated sample treated at voltage = 325 V for 5 min

The change in the lattice spacing d at different ψ angles resulted in a corresponding peak shift (Fig. 1), the measured 2θ is plotted as a function of $\sin^2 \psi$. The residual stress in the coating can be determined from Eq 1 and the linear slope of the fitted curve.

2.2.2 Microstructural Analyses. SEM (Quanta200 SEM, FEI, The Netherlands) was employed to observe the microstructures of the coatings. For sample preparation, the MgO coatings were sputter-coated with a thin layer of gold to minimize surface charging.

3. Results and Discussion

3.1 Phase Analyses

The XRD patterns of the MAO films formed at 250, 300, 325, and 350 V are shown in Fig. 2. It is indicated that the phase is mainly composed of Mg, MgO, $MgAl_2O_4$, and $Mg_3(PO_4)_2$. The Mg phase is from the AZ31 Mg alloy substrate.

At a low applied voltage (250 V), diffraction peak of MgO is very weak (Fig. 2a). Above this voltage, MgO peaks were identified clearly by XRD in each applied voltage. It is suggested that a cubic MgO can be obtained via regulating the applied voltage in the present electrolyte.

In addition, diffraction peaks of $MgAl_2O_4$ (spinel) were observed at all the applied voltages. The diffraction peak of $MgAl_2O_4$ is very strong at 250 V, and its intensity decreased when the applied voltage was increased. The presence of $Mg_3(PO_4)_2$ compounds suggested that the electrolyte ions participated in the growth process of the coating (Ref 22).

3.2 Microstructural Analyses

3.2.1 Surface Morphology. In Fig. 3, SEM observations revealed four types of surface morphology for the coatings produced at different voltages. As seen in Fig. 3(a), at the low voltage of 250 V, the oxidation coatings showed dense

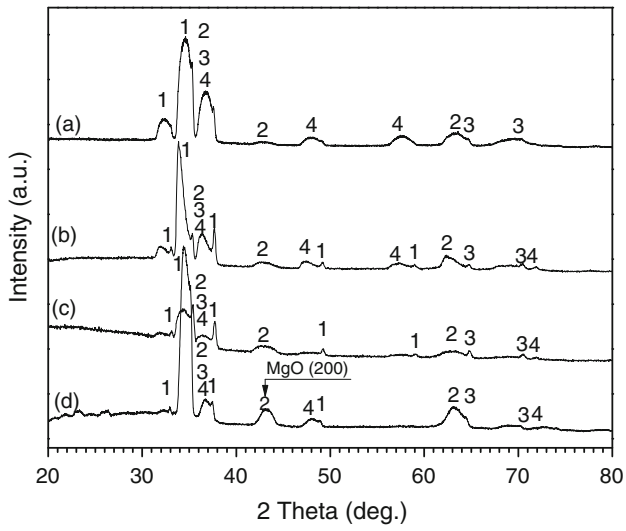

Fig. 2 XRD spectra of the MAO films at different voltages: (a) 250 V, (b) 300 V, (c) 325 V, and (d) 350 V (phase composition: 1, $Mg_3(PO_4)_2$; 2, MgO; 3, $MgAl_2O_4$; 4, Mg)

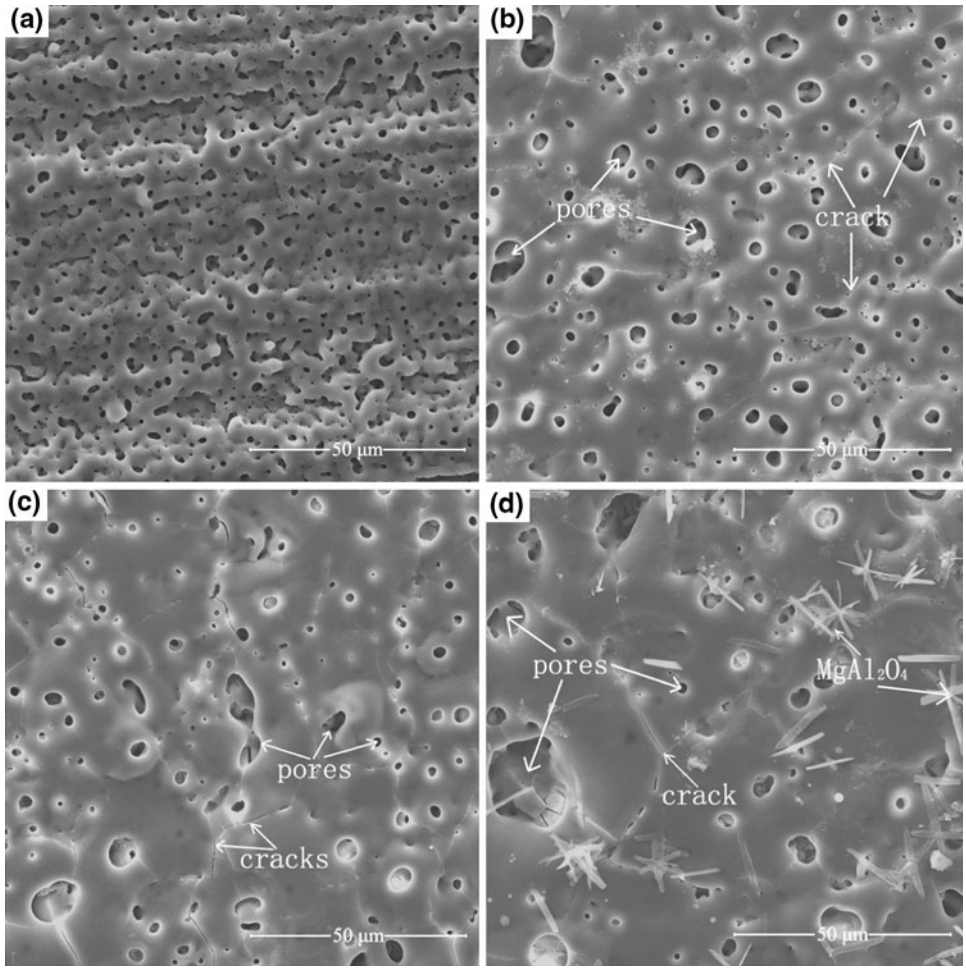

Fig. 3 Surface morphologies of the coatings at different applied voltages for 5 min: (a) 250 V, (b) 300 V, (c) 325 V, and (d) 350 V

crater-like microstructures with some round-shaped shrinkage pores in the crater centers for all the samples. Meanwhile, it was also noticed that a well-developed melt network was produced at 250 V.

As seen in Fig. 3(b), at a medium voltage 300 V, the s of the pores have increased. The large round- or elliptical-shaped pores imply the merger of small pores. In addition, many small cracks were evident in the coating.

At a voltage of 325 V (Fig. 3c), the number of larger and irregularly shaped micropores increased. Round- and elliptical-shaped pores and many small cracks were evident in the coating.

Finally, as shown in Fig. 3(d), a loose-grained, porous surface morphology with $MgAl_2O_4$ spinel crystals was observed for the coatings produced at the high voltage of 350 V. The sizes of the pores and cracks were dramatically bigger than those at 300 and 325 V, suggesting that the smaller pores were consumed and that large cracks were formed.

3.2.2 Cross-Sectional Morphology. Figure 4 shows the cross-sectional images of coatings coated with different voltages for 5 min. As seen in Fig. 4, micropores and microcracks were observed in the MAO-coated layers. These pores and cracks did not penetrate the entire coating layer. Yerokhin et al. (Ref 23) proposed that pores in the coating layer were produced from the gas bubbles thrown out of microarc discharge channels, while cracks were formed by thermal stress due to rapid solidification of the molten oxide in the relatively cold electrolyte.

In the general operating conditions, the coating formed on the AZ31 magnesium alloy was composed of three layers (Ref 12, 24): a 5-10 μm outer porous layer, a dense inner layer, and a thin contact layer between inner dense layer and metal substrate. The contact layer is relatively thin with a thickness of 100-300 nm. In our studies, as shown in Fig. 4(c), the inner layer of the MAO coating was relatively compact, while the outer layer had pores and tiny shrinkage holes. Figure 4(a) exhibited the smallest thickness because of the lowest voltage of 250 V, which resulted in an unobvious boundary between the substrate and the MAO coating. It can be noted that in the sample coated at 300 V (Fig. 4b), some larger microcracks and thicker layer were present than those observed in the sample coated at 250 V. The sample coated at 325 V showed relative uniform structure, compared with the other conditions (Fig. 4c). The sample coated at 325 V showed relatively uniform structure, compared with the other conditions (Fig. 4c). The coating thickness increased from 5 to 20 μm with increasing voltages from 250 to 350 V.

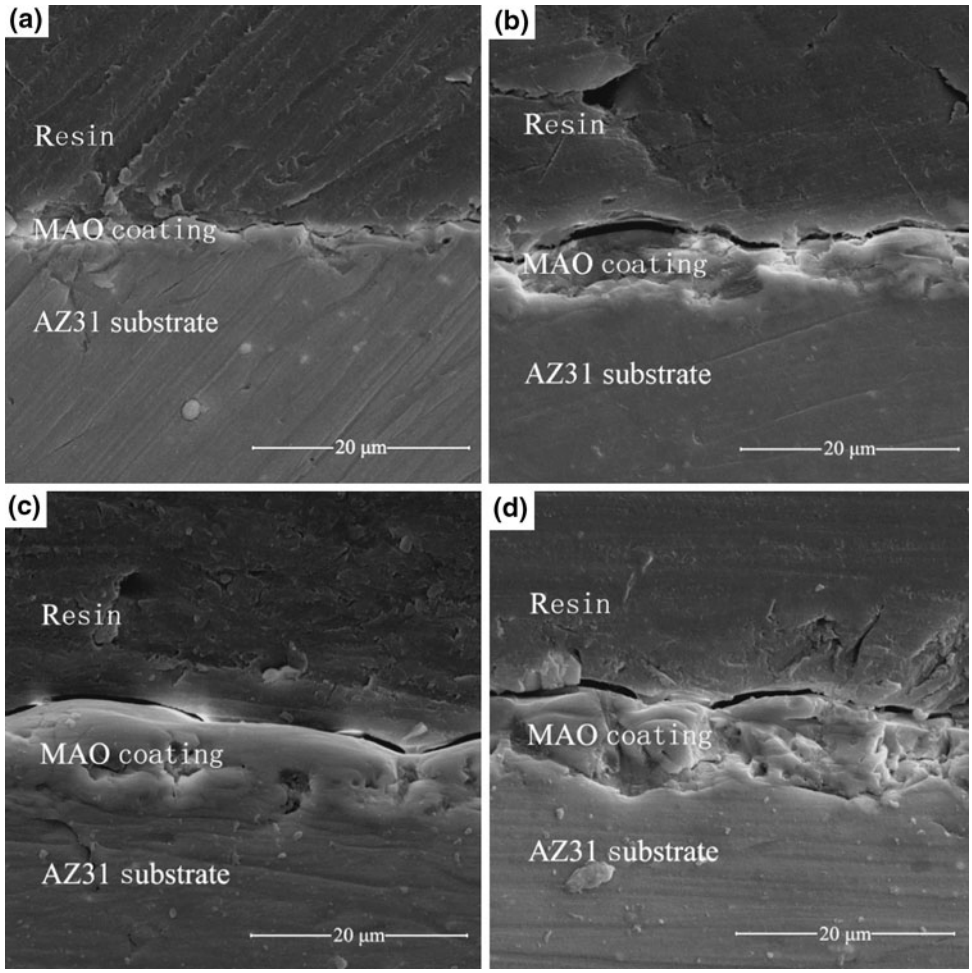

Fig. 4 Cross-sectional images of the coatings at different applied voltages for 5 min: (a) 250 V, (b) 300 V, (c) 325 V, and (d) 350 V

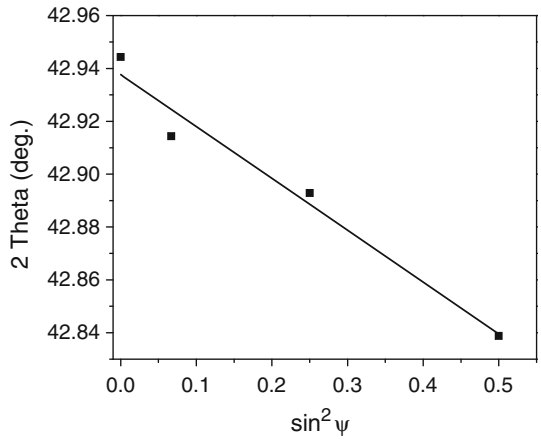

Fig. 5 An example of the plot 2θ vs. $\sin^2 \psi$ for the MAO-coated sample treated at voltage = 325 V for 5 min

3.3 Residual Stresses

The diffraction spectra for different ψ angles of MgO (200) are shown in Fig. 1. The sample tilt angle ψ is adopted as 0°, 15°, 30°, and 45°. Taking 2θ and $\sin^2 \psi$ as y-axis and x-axis, respectively, the XRD data are plotted in Fig. 5 from which the slope of the straight line is obtained by the least square fitting. The relationship between $\sin^2 \psi$ and the corresponding 2θ uses a linear fitting model (Eq 1).

Table 1 shows the related diffraction angle 2θ with different ψ angles for the MgO phase at different applied voltages. Based on Table 1 and Eq 1, residual stresses are calculated, the stress values obtained are shown in Table 2, and the curve of the residual stresses versus the applied voltages is plotted in Fig. 6.

As shown in Fig. 6 and Table 2, residual stresses evaluated for the samples at different applied voltages were found to be tensile and exhibited variance with voltages. With the increase of the applied voltages, stress values decreased. The highest residual stress was found to be 1418 MPa at the applied voltage of 250 V.

The decrease of residual stresses with increasing voltages is caused by the related microstructural change. The micropores produced by microarc discharge (see Fig. 3) could contribute to eliminating the residual stress. In this study, the pore size increases with increasing applied voltage. Large pores are formed at the expense of small ones, thereby reducing the residual stress. Additional reduction of stress is probably due to the formation of cubic MgO with the increase of the reaction energy, i.e., applied voltage. At lower applied voltage, the new generated phase structure (Fig. 2a, b) induces a mismatch with the alloy substrate (Ref 19), resulting in very high residual stress (Fig. 3a) during fast solidification of melts, when the film surface comes into contact with the solution. At higher voltage, the formation of cracks (Fig. 3b, c) could release residual stresses.

Table 1 The related diffraction angles 2θ with different sample tilt angles ψ for the MgO phase at different MAO applied voltages for 5 min

Applied voltage, V	ψ = 0°	ψ = 15°	ψ = 30°	ψ = 45°	$\frac{\partial(2\theta)}{\partial(\sin^2\psi)}$
250	42.67839	42.65392	42.59098	42.52551	−0.30546
300	42.85505	42.87670	42.82069	42.75057	−0.23611
325	42.94437	42.91434	42.89283	42.83878	−0.19628
350	43.06433	43.08570	43.03936	43.01857	−0.11730

Table 2 Residual stress values for the MgO phase at different MAO applied voltages

Applied voltage, V	250	300	325	350
Residual stress, MPa	1418	1096	912	545

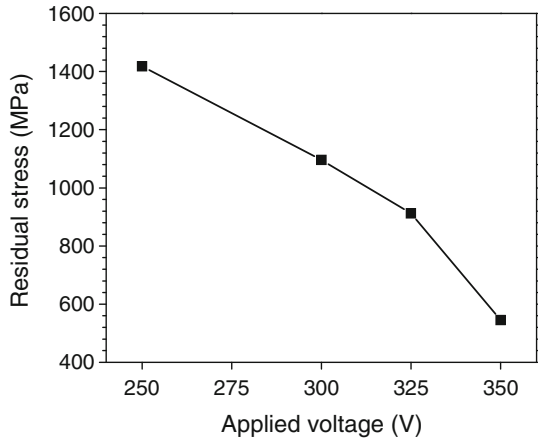

Fig. 6 Variations in residual stress at different applied voltages during MAO process treatment for 5 min

4. Conclusions

The residual stresses in MAO ceramic coatings on biocompatible AZ31 magnesium alloy were investigated using XRD as functions of applied voltages. The following results were obtained:

(1) The stresses measured by $\sin^2\psi$ XRD method in the MgO constituent of MAO coatings formed in diluted Na_3PO_4 have been found to be tensile in nature.
(2) The residual stresses decreased with the increase of the applied voltage. A MAO coating with uniform surface morphology and smaller residual stress was produced at 325 V. This condition can be considered as optimal for the range of process parameters studied in the present study.
(3) The micropores and cracks produced by microarc discharge could contribute to releasing the residual stresses.

Acknowledgments

The authors are grateful to Prof. Tom Trainor (the Department of Chemistry and Biochemistry of the University of Alaska Fairbanks) for providing the facilities for the x-ray diffraction analysis. JZ acknowledges the support of the NSF grant (award number 0723244). The study is supported by the UAF Graduate School Fellowship.

References

1. N.T. Kirkland et al., A Survey of Bio-Corrosion Rates of Magnesium Alloys, *Corros. Sci.*, 2010, **52**(2), p 287–291
2. M.P. Staiger, A.M. Pietak, J. Huadmai, and G. Dias, Magnesium and Its Alloys as Orthopedic Biomaterials: A Review, *Biomaterials*, 2006, **27**(9), p 1728–1734
3. R. Zeng, W. Dietzel, F. Witte, N. Hort, and C. Blawert, Progress and Challenge for Magnesium Alloys as Biomaterials, *Adv. Eng. Mater.*, 2008, **10**, p B3–B14
4. H. Wang, Y. Estrin, and Z. Zúberová, Bio-Corrosion of a Magnesium Alloy with Different Processing Histories, *Mater. Lett.*, 2008, **62**(16), p 2476–2479
5. W.-D. Mueller, M. Lucia Nascimento, and M.F. Lorenzo de Mele, Critical Discussion of the Results from Different Corrosion Studies of Mg and Mg Alloys for Biomaterial Applications, *Acta Biomater.*, 2010, **6**(5), p 1749–1755
6. M.A. Gonzalez-Nunez et al., A Non-Chromate Conversion Coating for Magnesium Alloys and Magnesium-Based Metal Matrix Composites, *Corros. Sci.*, 1995, **37**(11), p 1763–1772
7. Y. Mizutani et al., Anodizing of Mg Alloys in Alkaline Solutions, *Surf. Coat. Technol.*, 2003, **169–170**, p 143–146
8. H.M. Wong et al., A Biodegradable Polymer-Based Coating to Control the Performance of Magnesium Alloy Orthopaedic Implants, *Biomaterials*, 2010, **31**(8), p 2084–2096
9. T.M. Yue, A.H. Wang, and H.C. Man, Improvement in the Corrosion Resistance of Magnesium Composite by Excimer Laser Surface Treatment, *Scripta Mater.*, 1997, **38**(2), p 191–198
10. H. Hoche et al., Plasma Anodisation as an Environmental Harmless Method for the Corrosion Protection of Magnesium Alloys, *Surf. Coat. Technol.*, 2003, **174–175**, p 1002–1007
11. H. Altun and S. Sen, The Effect of DC Magnetron Sputtering AlN Coatings on the Corrosion Behaviour of Magnesium Alloys, *Surf. Coat. Technol.*, 2005, **197**(2–3), p 193–200
12. J.Y. Cho, D.Y. Hwang, D.H. Lee, B.Y. Yoo, and D.H. Shin, Influence of Potassium Pyrophosphate in Electrolyte on Coated Layer of AZ91Mg Alloy Formed by Plasma Electrolytic Oxidation, *Trans. Nonferrous Met. Soc. China*, 2009, **19**(4), p 824–828
13. H.P. Duan, K.Q. Du, C.W. Yan, and F.H. Wang, Electrochemical Corrosion Behavior of Composite Coatings of Sealed MAO Film on Magnesium Alloy AZ91D, *Electrochim. Acta*, 2006, **51**(14), p 2898–2908
14. R.F. Zhang, S.F. Zhang, and S.W. Duo, Influence of Phytic Acid Concentration on Coating Properties Obtained by MAO Treatment on Magnesium Alloys, *Appl. Surf. Sci.*, 2009, **255**(18), p 7893–7897
15. L. Zhao et al., Growth Characteristics and Corrosion Resistance of Micro-Arc Oxidation Coating on Pure Magnesium for Biomedical Applications, *Corros. Sci.*, 2010, **52**(7), p 2228–2234
16. M.D. Klapkiv, State of Electrolytic Plasma in the Process of Synthesis of Oxides Based on Aluminium, *Mater. Sci.*, 1995, **31**, p 494–499
17. E. Atar, C. Sarioglu, U. Demirler, E. Sabri Kayali, and H. Cimenoglu, Residual Stress Estimation of Ceramic Thin Films by X-Ray Diffraction and Indentation Techniques, *Scripta Mater.*, 2003, **48**(9), p 1331–1336
18. R.H.U. Khan et al., Residual Stresses in Plasma Electrolytic Oxidation Coatings on Al Alloy Produced by Pulsed Unipolar Current, *Surf. Coat. Technol.*, 2005, **200**(5–6), p 1580–1586

19. P. Huang, F. Wang, K.W. Xu, and Y. Han, Mechanical Properties of Titania Prepared by Plasma Electrolytic Oxidation at Different Voltages, *Surf. Coat. Technol.*, 2007, **201**(9–11), p 5168–5171
20. Y.C. Zhou, Z.Y. Yang, and X.J. Zheng, Residual Stress in PZT Thin Films Prepared by Pulsed Laser Deposition, *Surf. Coat. Technol.*, 2003, **162**(2–3), p 202–211
21. H. Heinrich and J.B. Mullin, *II-VI and I-VII Compounds; Semimagnetic Compounds*, Vol 41, Subvol B, Springer, 1999
22. K.L. Rama, K.R.C. Somaraju, and G. Sundararajan, The Tribological Performance of Ultra-Hard Ceramic Composite Coatings Obtained Through Microarc Oxidation, *Surf. Coat. Technol.*, 2003, **163–164**, p 484–490
23. A.L. Yerokhin et al., Plasma Electrolysis for Surface Engineering, *Surf. Coat. Technol.*, 1999, **122**(2–3), p 73–93
24. O. Khaselev, D. Weiss, and J. Yahalom, Structure and Composition of Anodic Films Formed on Binary Mg-Al Alloys in KOH-Aluminate Solutions Under Continuous Sparking, *Corros. Sci.*, 2001, **43**(7), p 1295–1307